Article

Molecular and Crystal Structure of a Chitosan−Zinc Chloride Complex

Toshifumi Yui [1],* , **Takuya Uto [2]** and **Kozo Ogawa [3]**

1   Faculty of Engineering, University of Miyazaki, Nishi 1-1 Gakuen-kibanadai, Miyazaki 889-2192, Japan
2   Organization for Promotion of Tenure Track, University of Miyazaki, Nishi 1-1 Gakuen-kibanadai, Miyazaki 889-2192, Japan; t.uto@cc.miyazaki-u.ac.jp
3   Research Institute for Advanced Science and Technology, Osaka Prefecture University, 1-2 Gakuencho, Sakai, Osaka 599-8570, Japan; ogawakt@kawachi.zaq.ne.jp
*   Correspondence: tyui@cc.miyazaki-u.ac.jp; Tel.: +81-985-58-7319

Abstract: We determined the molecular and packing structure of a chitosan–$ZnCl_2$ complex by X-ray diffraction and linked-atom least-squares. Eight D-glucosamine residues—composed of four chitosan chains with two-fold helical symmetry, and four $ZnCl_2$ molecules—were packed in a rectangular unit cell with dimensions a = 1.1677 nm, b = 1.7991 nm, and c = 1.0307 nm (where c is the fiber axis). We performed exhaustive structure searches by examining all of the possible chain packing modes. We also comprehensively searched the positions and spatial orientations of the $ZnCl_2$ molecules. Chitosan chains of antiparallel polarity formed zigzag-shaped chain sheets, where N2···O6, N2···N2, and O6···O6 intermolecular hydrogen bonds connected the neighboring chains. We further refined the packing positions of the $ZnCl_2$ molecules by theoretical calculations of the crystal models, which suggested a possible coordination scheme of Zn(II) with an O6 atom.

Keywords: chitosan−$ZnCl_2$ complex; crystal structure; X-ray fiber diffraction

1. Introduction

Chitin—a linear polysaccharide composed of β-(1→4)-linked *N*-acetyl-D-glucosamine monomers—is the most abundant and renewable natural polymer after cellulose. One commonly finds chitin in the exoskeleton or cuticles of many invertebrates, and the cell walls of most fungi and some algae. Recently, chitinous skeletal fibers from some marine demosponges were attracted attention as a possible application to scaffolds for cultivation [1]. Chitosan, a partially or fully deacetylated derivative of chitin, exhibits a regular distribution of aliphatic primary amino groups and primary hydroxyl groups. Unlike its corresponding parent polymer, chitosan is soluble in various aqueous acids and has a remarkable ability to form specific complexes with a number of ions, such as transition and post-transition metal ions [2,3]. Chitosan is a unique cationic biopolymer that is available in large quantities. Researchers have commercialized it as follows: a coagulant for wastewater, animal feed, fertilizer, an antibacterial additive for clothing, and a precursor for glucosamine [4]. Chitosan is conventionally a powder or a film, yet chitosan nanofibers—typically fabricated by electrospinning—are an active area of research. Researchers have used electrospun nanofibers of chitosan—and corresponding blends with other polymers—for separations, as biological scaffolds, and for drug delivery [5–7]. Researchers have also used electrospun chitosan nanofibers to remove low concentrations of metal ions [8] and arsenate ions [9] from water.

Researchers first obtained the X-ray fiber pattern of chitosan—by solid-state deacetylation of a lobster tendon—in a hydrated crystalline form [10]. The results indicated a two-fold helical symmetry for chitosan as a molecular chain structure in a similar manner as chitin. Researchers first obtained the other polymorph of chitosan, an anhydrous form, by annealing the following: a stretched chitosan sample at ≥190 °C in water [11], and

a crab tendon chitosan in water at ~240 °C [12]. The reported crystal structures of both the hydrated and anhydrous forms are in atomistic detail, as per analyses of corresponding X-ray diffraction data [12–14]. Researchers reported further structural details of the anhydrous form—such as the positions of the hydroxyl and amino hydrogen atoms—by using periodic density functional theory (DFT), which indicated a possible scheme of the hydrogen bond network [15]. The structures of chitosan metal complexes and salts are also pertinent. Researchers have proposed two types of coordination mode: the pendant model [16,17] and the bridge model [18]. The chitosan–HI salt, the only chitosan complex for which there is a crystal structure in atomistic detail, involves two independent iodide ions: one coordinated with three amino groups, and one that accepts one hydrogen atom from an amino group and two hydrogen atoms from the O6 hydroxyl groups [19]. This may be interpreted as a hybrid of the bridge and pendant coordination modes, in terms of interactions with the amino groups. However, the coordination structures of chitosan–metal complexes remained unsolved.

Ogawa et al. reported an X-ray diffraction study of crab tendon chitosan samples complexed with Cd(II), Zn(II), and Cu(II) salts; the $ZnCl_2$ complex sample provided a fiber diffraction pattern of higher quality compared with the other chitosan metal salts [20]. The affinity of chitosan for Zn cations can be pertinent to applications. For example, regarding wastewater treatment, chitosan exhibits a medium affinity for Zn(II) compared with other divalent metallic ions—approximately one-third that for Cu(II) and almost equivalent to that for Cd(II), which enabled a chitosan film to remove zinc ions up to ~50% of the initial concentration in the effluent [21]. The chitosan–Zn complex exhibited broad-spectrum antimicrobial activities, especially against *Escherichia coli* [22]. Researchers incorporated a zinc electrodeposit—applied on a steel construction surface for protection and as a barrier against corrosion—with chitosan to form chitosan–zinc composite electrodeposits with enhanced antibacterial properties [23]. Nanoscale fabrication of chitosan further enhances these functionalities of zinc complexes.

In the present study, we determined and analyzed the crystal structure of a chitosan–$ZnCl_2$ complex to reveal the coordination structure of the zinc ion by X-ray fiber diffraction, which we combined with molecular mechanics (MM) and quantum mechanical modeling. The final crystal structure that the molecular chains arranged to form zigzag-shaped chain sheets along the *a*-axis, where the neighboring chains were connected by intermolecular hydrogen bonds involving the N2 and O6 atoms. $ZnCl_2$ molecules were located at the bending positions of the chain sheets. Although no clear coordinate bond with an amino group was detected, O6–H···Zn(II) coordinate bonds were suggested in the semi-empirical quantum mechanics (SEQM)-optimized crystal model.

2. Materials and Methods

2.1. Sample Preparation and X-ray Diffraction

Our method of obtaining X-ray fiber diffraction data was described in our previous study [16,20]. Briefly, tendon chitosan was prepared from a highly oriented chitin specimen of a crab tendon, *Chionecetes opilio* O. Fabricius, by *N*-deacetylation with 67% aqueous sodium hydroxide at 100 °C for 2 h under a nitrogen atmosphere. The degree of *N*-acetylation of the tendon chitosan was found to be 0% by measurement of a colloidal titration, and the viscosity average polymerization was 10,800 [16,20]. The tendon chitosan was soaked in aqueous $ZnCl_2$. The X-ray fiber diffraction patterns were recorded with a box camera equipped with an imaging plate (Fujifilm HR-III), at 76% relative humidity in a helium atmosphere, with a Rigaku Geigerflex diffractometer equipped with Ni-filtered Cu Kα radiation. The X-ray diffraction image was read with an imaging plate detector (Rigaku R-AXIS), and the three-dimensional intensity profile was analyzed with Surfer (Golden Software, Inc., Golden, CO, USA) for resolution of overlapped profiles, background removal, and calculations of peak intensities. A set of the measured intensities was corrected for the Lorentz and polarization factors to provide a set of observed structure factors, F_o.

The density of the tendon chitosan–ZnCl$_2$ complex was measured by flotation with a carbon tetrachloride–*m*-xylene solution.

2.2. Crystal Structure Analysis

Figure 1 shows the principal parameters to describe chitosan chain conformation and position in the unit cell, together with atom labeling. A molecular chain structure with two-fold helical symmetry was the observed form of the chitosan crystal structures and was not substantially changed throughout structure refinement except in terms of the orientations of the hydroxymethyl groups, χ_{O6}, which were defined by the O5–C5–C6–O6 sequence. The conformation usually prefers three staggered positions, which was termed as either *gauche–trans* (*gt*), *gauche–gauche* (*gg*), or *trans–gauche* (*tg*); the χ_{O6} values of the respective positions are 60°, −60°, and 180°. The positions of the ZnCl$_2$ molecules were associated with the primary amino groups of the glucosamine residues and were defined by a set of internal coordinates: the N2–Zn distance, $d_{N2–Zn}$; the C2–N2–Zn angle, θ_{Zn}; the rotation of the C1–N2 bond, χ_{Zn}; the N1–Zn–Cl1 angle, θ_{Cl1}; and the rotation of N2–Zn, χ_{Cl1}. The torsion angles, χ_{Zn} and χ_{Cl1}, were defined by the atom sequences of C1–C2–N2–Zn and C2–N2–Zn–Cl1, respectively. The initial position of the other chlorine atom, Cl2, was defined by reporting 180° as the Cl1–Zn–Cl2 angle, such that the ZnCl$_2$ molecule of an initially linear structure could bend in either direction during structure refinement.
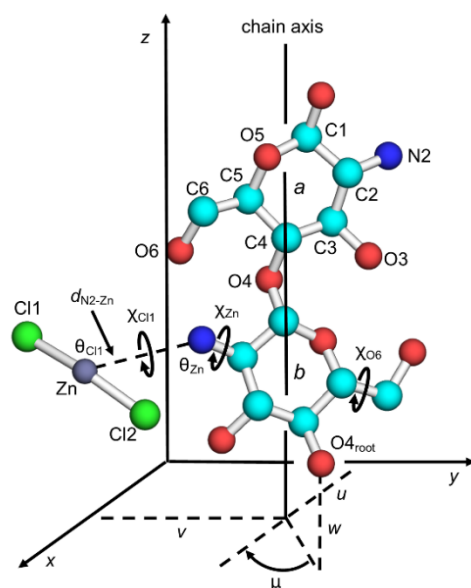

Figure 1. Two-fold helix structure of chitosan together with atom and residue designations. Notation is as follows: chain packing parameters (μ, *u*, *v*, and *w*), hydroxymethyl conformation (χ_{O6}), and ZnCl$_2$ position parameters (χ_{Zn}, χ_{Cl1}, θ_{Zn}, θ_{Cl1}, and $d_{N2–Zn}$).

The chain positions in the crystal unit cell were defined by the chain packing parameters: the chain rotational position, μ in degrees, with respect to the helix axis; and the chain translational positions, *u*, *v*, and *w*, in fractions, along the *a*, *b*, and *c* dimensions, respectively. Whereas the *u* and *v* parameters define the position of the helix axis on the *ab* base plane, the μ and *w* parameters correspond to the positions of the root atom, O4$_{root}$, in Figure 1; μ = 0° and *w* = 0 when O4$_{root}$ is at (x, 0, 0) for a helix origin.

Molecular and packing structures—of chitosan chains and ZnCl$_2$ molecules—were determined by using the linked-atom least-squares (LALS) program [24,25], where the quantity Ω was minimized as per the following:

$$\Omega = \sum_m w_m \left(|F_{m,o}|^2 - k^2 |F_{m,c}|^2 \right) + s \sum_{i,j} \epsilon_{i,j} + \sum_q \lambda_q G_q \tag{1}$$

The first summation term ensures optimum agreement between the observed ($F_{m,o}$) and calculated ($F_{m,c}$) X-ray structure amplitudes of the *m*-th reflection. Term *k* is a scaling factor. The weight of the reflection, w_m, was fixed to 1.0 for observed reflections, 0.5 for unobserved reflections in which $F_{m,c} > F_{m,o}$, and 0.0 for unobserved reflections in which $F_{m,c} < F_{m,o}$. The second summation term evaluates non-bonded repulsions between atoms *i* and *j*. The quantity *s* is an overall weight of the non-bonded repulsions. The third summation term imposes the atomic coordinate constraints by the method of Lagrange undermined multipliers. The constraints were adopted to preserve helix continuity and pyranose ring closure of the residue. The overall agreement between the observed and calculated X-ray structure amplitudes was evaluated by a weighed residual:

$$R_w = \frac{\sum_m w_m (|F_{m,o}| - |F_{m,c}|)^2}{\sum_m w_m F_o^2} \tag{2}$$

The unobserved reflections below the observable threshold were included in calculating both Equations (1) and (2). One-half of the minimum intensity was assigned to estimate the magnitude of F_o for unobserved reflections.

2.3. Theoretical Calculations of Crystal Models

A theoretical study of crystal models with finite dimensions was carried out to refine orientations of the hydroxyl, hydroxymethyl, and amino groups and the positions of the $ZnCl_2$ molecules. Two crystal models, differing in the constituent number of the chitosan chains, were constructed on the basis of the crystal structure determined by X-ray analysis: chitohexaose × 25 and chitohexaose × 9. Both models considered four $ZnCl_2$ molecules in the inner core, which enabled the $ZnCl_2$ molecules to exist in a crystalline state. Partial structure optimizations were applied to the crystal models, such that the three substituent group orientations and the $ZnCl_2$ positions were allowed to vary, whereas the backbone structures of chitohexaose were static. MM was applied to optimizations of the chitohexaose × 25 models by using a universal force field (UFF) [26] where the atomic charges were assigned by charge equilibration [27]. Researchers have applied a UFF to MM calculations involving metal complexes [27–29]. Optimizations of the chitohexaose × 9 models were performed by using SEQM with a PM6 Hamiltonian [30]. Tight convergence self-consistent field criteria (10^{-8} a.u.) were applied in the SEQM optimizations. The accuracy of the PM6 Hamiltonian for Zn(II) complexes was demonstrated by systematic benchmarks [30,31]. Its reliability was also reported for crystal structure studies of proteins and other organic materials with complexes of Zn(II) [32–34]. All of the MM and SEQM calculations were performed by using Gaussian 09 Rev. C01 [35].

2.4. Visualizations of Crystal Structures

Molecular graphics software, PyMOL 1.7.1, was used to visualize and draw the crystal structures [36].

3. Results and Discussion

3.1. Crystal Data

Figure 2 shows an X-ray fiber diffraction pattern of the chitosan–$ZnCl_2$ complex. We indexed a total of 33 observed diffraction spots up to the fourth layer with a rectangular unit cell, dimensions *a* = 1.1677 nm, *b* = 1.7991 nm, and *c* =1.0307 nm (where *c* is the fiber axis). Table S1 shows the observed and calculated *d*-spacings. The unit cell accommodated eight glucosamine units—comprised of four chitosan chains with a two-fold helical conformation, and four $ZnCl_2$ molecules—resulting in a calculated density ρ_{calc} = 1.41 g/cm^3. One can insert an additional 16 water molecules into the unit cell, resulting in ρ_{calc} = 1.63 g/cm^3, for a better fit to the observed density, ρ_{obs} = 1.56 g/cm^3.
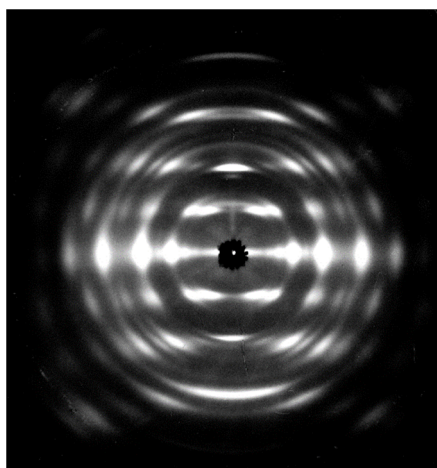
Figure 2. X-ray fiber diffraction pattern of the chitosan–ZnCl$_2$ complex.

3.2. Search for Chain Packing Structures

Researchers have proposed that chitosan chains are packed with $P2_12_12_1$ symmetry in the parent crystal structures of both the anhydrous chitosan and chitosan hydrate crystal structures, where the positioning of a pair of neighboring chains in antiparallel polarity is related by two-fold helical symmetry along either the *a* or *b* axis [12–14]. Similarly, we assumed involvement of two-fold helical symmetry to generate antiparallel chain pairs, despite the fact that we observed odd reflections on *h*00 and 0*k*0, such as 100 and 070, in the fiber diagram. We rationalized such violation of systematic absences by non-symmetrical packing of ZnCl$_2$ molecules. We assumed two types of space groups, $P2_1/a$ and $P2_1/b$, to define a chain packing structure in the unit cell. The space group models required two independent chains, each consisting of two consecutive glucosamine units as an asymmetric unit. We defined the eight chain packing models by a combination of the space group, chain positions, and chain polarities for the two independent chains (Table 1). For each of the chain packing models, we considered the three staggered positions of the hydroxymethyl group (*gt*, *gg*, and *tg*) to give 24 initial structures. For all eight glucosamine residues, we linked a ZnCl$_2$ molecule to an amino group with an initial $d_{N2–Zn}$ of 0.22 nm, whereas we set the occupancy of Zn and Cl atoms to be 0.5, and thus the number of ZnCl$_2$ molecules was effectively four, instead of eight.

Table 1. Chain packing modes of chain packing models.

Model	Chain Positions		Chain Polarities [1]	
	Chain 1 (*u*1, *v*1)	Chain 2 (*u*2, *v*2)	Chain 1	Chain 2
$P2_1/a$ space group				
1	0.0, 0.0	0.0, 0.5	up	up
2			up	down
3	0.25, 0.25	0.25, 0.75	up	up
4			up	down
$P2_1/b$ space group				
5	0.0, 0.0	0.5, 0.0	up	up
6			up	down
7	0.25, 0.25	0.25, 0.75	up	up
8			up	down

[1] When the position of C1 is higher than that of C4 along the fiber axis, a chain polarity is up. Otherwise, a chain polarity is down.

The first stage of the chain packing structure search was to determine the appropriate *ab* projection structures based on the *F*(*hk*0) data for the initial 24 structures. The values of $\mu1$ and $\mu2$ were stepped from a value of 0° to a value of 180° by 10° increments to provide two-dimensional R_w maps. We generally found the R_w minima at approximately ($\mu1$, $\mu2$) = (0°, 0°), (0°, 90°), (90°, 0°), and (90°, 90°) in most of the 24 R_w maps. On the basis of the results of the $\mu1$–$\mu2$ search, we generated 432 initial structures by combining six $\mu1$ and $\mu2$ values (–10°, 0°, 10°, 80°, 90°, and 100°), three χ_{O6} values (60°, –60°, and 180°), two χ_{Zn} values (–60° and 120°), and two χ_{Cl1} values (0° and 90°); and refined the structures with respect to the $\mu1$ and $\mu2$ values. Among the 432 $\mu1$–$\mu2$ refined structures, we selected that which exhibited the lowest R_w value to represent each of the chain packing models (Table S2). As a result, chain packing model 2 clearly differed from the other models by its comparatively low R_w values. Table 2 shows the final R_w values of the three models of chain packing model 2, all of which were adopted to search for an appropriate N2–Zn distance, d_{N2-Zn}. Because LALS sets bond length as a non-variable parameter, we carried out the d_{N2-Zn} search by stepping the d_{N2-Zn} value from a value of 0.22 nm to a value of 5.0 nm in 0.01-nm increments, whereas we varied the parameters $\mu1$, $\mu2$, χ_{O6}, χ_{Zn}, χ_{Cl1}, and θ_{Zn}. Table 2 shows the R_w values at the minima with respect to the d_{N2-Zn} change, and the corresponding d_{N2-Zn} values.

Table 2. Summary of *ab* projection structure analysis.

Hydroxymethyl Conformation	R_w (d_{N2-Zn} in nm)			
	μ1-μ2 refinement			
gg	0.310 (0.22)			
gt	0.289 (0.22)			
tg	0.290 (0.22)			
	d_{N2-Zn} search			
gg	0.192 (0.23)	0.392 (0.36)	0.302 (0.45)	
gt	0.185 (0.25)	0.150 (0.30)	0.199 (0.37)	0.208 (0.45)
tg	0.214 (0.23)	0.196 (0.40)	0.202 (0.46)	

We then focused our crystal structure analysis on three-dimensional chain packing structure searches using the higher-layers *F*(*hkl*) data, where $l = 1 - 3$, in addition to the *F*(*hk*0) data. For each of the 10 refined models (Table 2), we stepped the chain translational positions ($w1$ and $w2$) from a value of –0.4 to a value of 0.5 in increments of 0.1, which generated 100 structures with respect to the $w1$–$w2$ positions. We varied the $w1$ and $w2$ values, and the angle parameters θ_{Zn}, in addition to the parameters in the previous d_{N2-Zn} search. We selected the three-dimensional chain packing structure with the lowest R_w value from the 100 refined structures. Among the remaining 10 models, we screened three (d_{N2-Zn} = 0.30, 0.37, or 0.46 nm) for the next crystal structure refinement stage. Table 3 shows the final R_w values and the refined chain packing parameters of the three selected models. Although the initial hydroxymethyl conformations were *gt* for models 1 and 2, and *tg* for model 3 (Table 3), most of the χ_{O6} angles substantially rotated into different conformers compared with the original conformations.

Table 3. Chain packing parameters and R_w values of models selected in three-dimensional structure search.

Model	R_w	d_{N2-Zn}	Chain Packing Parameters			
			μ1 (deg.)	*w1* (frac.)	μ2 (deg.)	*w2* (frac.)
1	0.259	0.30	−11.7	0.068	116	−0.108
2	0.258	0.37	−2.91	−0.053	109	−0.174
3	0.245	0.46	−4.78	−0.214	109	−0.138

3.3. Crystal Structure Refinement by Combined X-ray Data and Stereochemical Constraints

We performed the final stage of crystal structure analysis mainly to refine the $ZnCl_2$ packing positions. We introduced the stereochemical constraints, the second term of Equation (1), to suppress development of unrealistically short contacts between nonbonding atoms during structure refinement. We excluded a hydroxymethyl conformation, χ_{O6}, from two-fold helical symmetry operation of the chain, which allowed four χ_{O6} parameters—corresponding to the two independent chains—to rotate independently. In the structure refinement stage, we set the occupancy of a $ZnCl_2$ molecule to be 1.0, such that the two amino groups were linked to the two respective $ZnCl_2$ molecules and the remaining two remained unlinked, which required six linking patterns of $ZnCl_2$ molecules (Figure S1). We allowed two sets of the $ZnCl_2$ position parameters (χ_{Zn}, χ_{Cl1}, and θ_{Zn}) to independently vary, and we stepped the remaining $ZnCl_2$ position parameter (d_{N2-Zn}) from a value of 0.27 nm to a value of 0.47 nm in 0.01 nm increments. At each d_{N-Zn} position, we generated 1296 initial structures by combining four sets of three χ_{O6} values (60°, −60°, and 180°), two sets of two χ_{Zn} values (−60° and 120°), and two sets of two χ_{Cl1} values (0° and 90°); whereas we used the initial chain packing positions ($\mu 1$, $\mu 2$, $w1$, and $w2$) from either of the three selected models (Table 3), depending on the d_{N2-Zn} value. We carried out full minimization of the Ω function of Equation (1) with respect to all of the parameters previously discussed. Figure 3 shows the adiabatic R_w changes for the six $ZnCl_2$ linking pattern models with respect to the d_{N2-Zn} value, where we used the R_w values from the refined structures corresponding to the lowest R_w values among the 1296 possible values. The R_w values decreased in accordance with increasing d_{N-Zn}, accompanied by several minima, suggesting that the $ZnCl_2$ molecule preferentially intercalated between the chitosan chains rather than closely coordinated to a particular primary amino group. Table 4 shows the chain packing parameters (μ and w), R_w, and contact σ, the second summation term of Equation (1) representing a magnitude of short nonbonding contact, for the final seven structures, which we selected on the basis of the threshold R_w value of 0.245 (defined arbitrarily). Considering the fact that there were negligible differences in the R_w values among the seven final structures, we selected model 4 because it corresponded to the smallest contact σ value corresponding to a comparatively low R_w value.
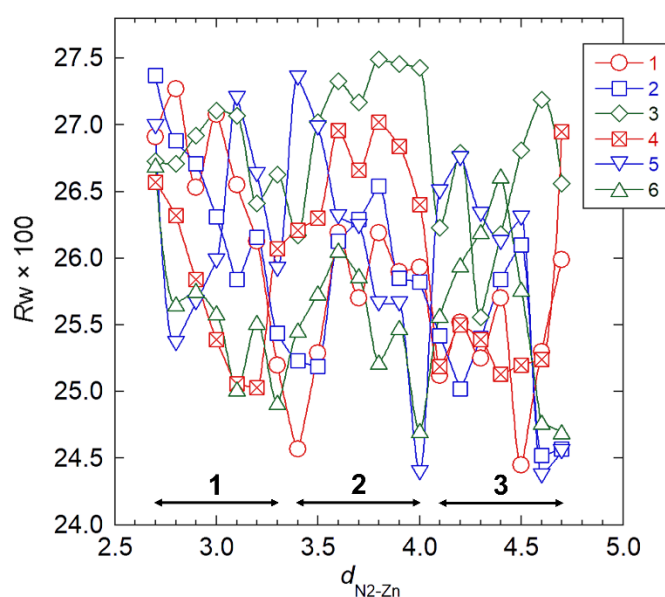

Figure 3. R_w with the respect to N2–Zn distance, d_{N2-Zn}, in structure refinement for six $ZnCl_2$ linking patterns. Double-headed arrows indicate d_{N2-Zn} ranges where we obtained the models by the preceding three-dimensional structure refinement. Numbers 1–6 refer to corresponding model numbers.

Table 4. Chain packing parameters, R_w, and nonbonding contacts of final refined models.

Model	ZnCl$_2$ Linking Pattern	Contact σ	R_w	d_{N2-Zn} (nm)	μ1 (deg.)	w1 (frac.)	μ2 (deg.)	w2 (frac.)
					Chain Packing Parameters			
1	1	83	0.246	0.34	3.61	−0.119	102	−0.243
2	5	138	0.244	0.40	−4.07	−0.116	106	−0.215
3	6	147	0.247	0.40	−0.402	−0.063	102	−0.209
4	1	52	0.245	0.45	12.1	−0.388	103	−0.345
5	2	172	0.245	0.46	11.5	−0.230	102	−0.169
6	5	193	0.244	0.46	−2.84	−0.214	107	−0.168
7	6	151	0.247	0.47	−2.02	−0.215	111	−0.154

We performed an additional full optimization run for model 4, where we introduced the angle parameter, θ_{Cl1}, to allow ZnCl$_2$ molecules to form a bent structure; we increased the magnitude of an overall weight of the non-bonded repulsions, s, in Equation (1) by 5× that which we adopted in the preceding runs to remove excessive non-bonding repulsions. Table 5 shows the values of the representative parameters of the final structure, and Figure 4 shows the structure's projections. Table S3 shows the coordinates of the final structure, and Table S4 shows the observed and calculated structure factor amplitudes.

Table 5. Representative parameters of the final structure.

Hydroxymethyl Conformations, χ_{O6}		
Labels	Chain No.	Values (deg.)
χ_{O6A}	1, 2	171
χ_{O6B}	1, 2	170
χ_{O6A}	3, 4	171
χ_{O6B}	3, 4	84.8

Chain Packing Parameters, μ and w		
Labels	Chain no.	Values
μ1/deg.	1, 3	14.01
w1/frac.	1, 3	−0.3853
μ2/deg.	2, 4	102.1
w2/frac.	2, 4	−0.3431

Distances of Intramolecular Hydrogen Bond		
Atom Labels		Values (nm)
O3a/b	O5a/b	0.272

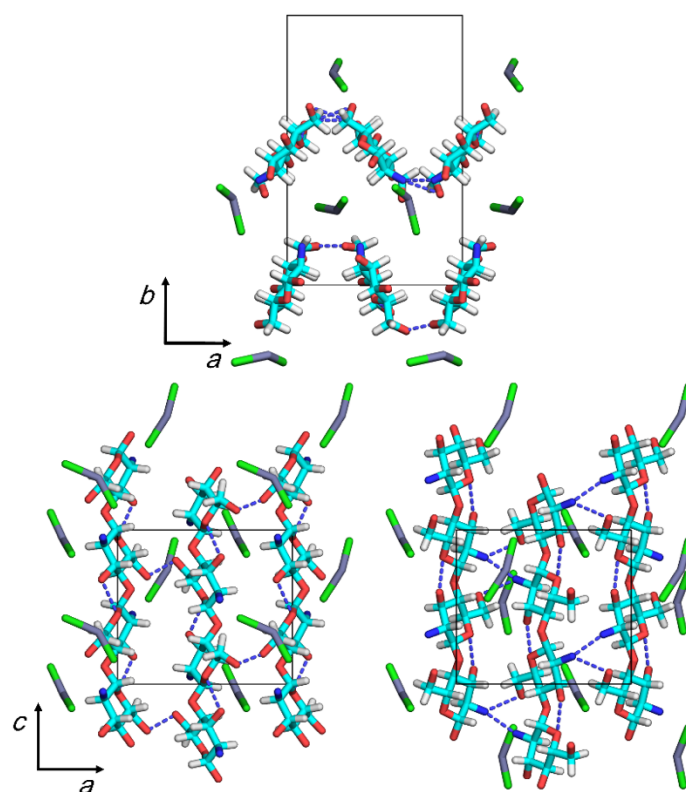| Distances of Intermolecular Hydrogen Bonds				
Atom Labels	Chain No.	Atom Labels	Chain No.	Values (nm)
O6a	1	O6b	2	0.198
O6b	1	O6a	2	0.220
O6a	3	N2a	4	0.285
N2b	3	N2a	4	0.256
O6b	3	N2b	4	0.286
N2a	3	O6a	4	0.285
N2a	3	N2b	4	0.256
		R_w		0.247
		contact σ		39

Figure 4. Projections of the proposed crystal structure on the *ab* (top) and *ac* (bottom) base planes (left: the chain sheet consisting of chains 1 and 2; right: the chain sheet consisting of chains 3 and 4). Dashed lines indicate hydrogen bonds.

Although the final R_w value increased slightly at the expense of a decreasing contact σ value, the short contact between an N2a atom in chain 3 and a Cl atom of the $ZnCl_2$–3 molecule remained, resulting in a distance of 0.22 nm. The N2 and O6 atoms participated in intermolecular hydrogen bonding to form chain sheets that exhibited a zigzag shape along the *a*-axis. The distances of O6a⋯O6b intermolecular hydrogen bonds, ~0.2 nm, involved the chain 1–2 sheets, possibly indicating the presence of short contacts in the atom pairs rather than hydrogen bonds. The other intermolecular hydrogen bonds in the chain 3–4 sheets formed with an optimum distance of ~0.28 nm. $ZnCl_2$ molecules were located around the bending portions of the chain sheets. The molecules were simply intercalated between the chain sheets and did not clearly coordinate to any particular amino or hydroxyl group nearby.

3.4. Theoretical Calculations of Crystal Models

We examined the crystal structure by using theoretical calculations implemented by MM and in accordance with SEQM methods, to refine the positions of the $ZnCl_2$ molecules as a primary objective. We performed the first MM calculations to search for preferred orientations of the hydroxyl and amino groups. Combining three staggered positions of the two hydroxyl groups on the C2 and C6 atoms, and those of the amino group, for each of the eight independent glucosamine units generated 6561 initial structures of the 25×hexaose model. We initially set the C3 hydroxyl group to be C2–C3–O3–H at *trans*, which formed an O3–H⋯O5 intramolecular hydrogen bond commonly observed in the parent chitosan crystal structures [12,13]. We partially optimized the structures of the 25×hexaose models, where the backbone structures of the chitosan chains were static, whereas we allowed the following to change: the orientations of the hydroxyl, amino, and hydroxymethyl groups; and the positions of the $ZnCl_2$ molecules. We selected 100 structures in terms of the lowest total steric energy and transferred their structural features (the substituent

orientations and ZnCl$_2$ positions) to the 9 × hexaose models, which we then subjected to SEQM partial structure optimization. Figure 5 shows the *ab* projection of the lowest structure obtained by SEQM calculations. Compared with the starting crystal structure, the molecular axes of the ZnCl$_2$ molecules were more aligned with the fiber axis, whereas the Zn atoms had not moved appreciably from their initial positions. They had slightly bent to give Cl1–Zn–Cl2 angles of 147° and 152°, respectively, and the corresponding Zn atoms were coordinated by the adjacent O6–H groups, with N2–O6 distances of 0.22 and 0.24 nm, respectively. The DFT study of the D-glucosamine–ZnCl$_2$ complex models predicted the length of the coordinate bond between a glucosamine residue and a ZnCl$_2$ molecule to be ~0.20 nm [37]. The hydrogen-bonding network suggested for the crystal structure was found mostly conserved in the SEQM-optimized structure, where the amino groups served as hydrogen donors to the O6–H groups. Unfortunately, we observed all of the 100 SEQM-optimized structures—as per structure amplitudes—to give unacceptable R_w values of ~0.5. A possible interpretation for the considerable disagreement between the X-ray data and SEQM-optimized structure is that ZnCl$_2$ molecules, in the presence of water molecules, may partly dissociate in the chitosan–ZnCl$_2$ crystal structure. The crystal structures derived from concentrated ZnCl$_2$ solutions depend on complete coordination of Cl$^-$ and H$_2$O around Zn^{2+} [38]. In the crystal structure of ZnCl$_2$·2.5H$_2$O, for example, one Zn^{2+} involved a tetrahedral coordination with Cl$^-$, and the other Zn^{2+} resided in the octahedral environment defined by five H$_2$O molecules and one Cl$^-$ shared with [ZnCl$_4$]$^{2-}$ [38].
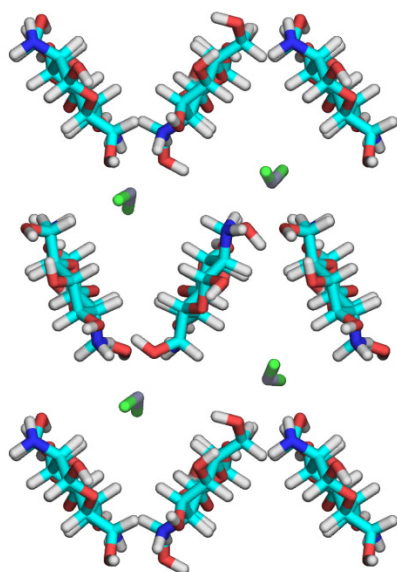

Figure 5. Projections of the SEQM-optimized structure of the crystal model on the *ab* base planes.

4. Conclusions

We reported atomistic detail of a chitosan–ZnCl$_2$ crystal structure. The molecular chains arrange to form zigzag-shaped chain sheets along the *a*-axis, where the neighboring chains in antiparallel polarity—related by two-fold helical symmetry along the same axis—are connected by intermolecular hydrogen bonds involving the N2 and O6 atoms. ZnCl$_2$ molecules are located at the bending positions of the chain sheets. The features are substantially similar to those detected in the crystal structure of chitosan–HI salt [19], suggesting that the features are likely common among chitosan–metal and chitosan–salt complexes. Although we did not detect a clear coordinate bond in the present crystal structure, a minor adjustment of the hydroxymethyl substituent structure may correspond to O6–H···Zn(II) coordinate bonds, in accordance with the structural features of the SEQM-optimized crystal model. It is possible that there is more stable complexation in the crystal structure involving dissociated Zn^{2+} and Cl$^-$ ions, as well as H$_2$O molecules, resulting

in Zn(II) that is readily accessible to the amino and hydroxyl groups. Two-fold helical symmetry—introduced to the present structure analysis because of technical reasons—restricted the diversity of the molecular packing, likely preventing glucosamine residues and ZnCl$_2$ molecules from complex formation. Extension to a complete *P*1 symmetry analysis may require one to investigate a large number of structural parameters and X-ray diffraction data obtained at higher resolution.

Supplementary Materials: The following are available online at https://www.mdpi.com/article/10.3390/nano11061407/s1, Figure S1: Six ZnCl$_2$ linking patterns for two independent chains; Table S1: Calculated and observed *d*-spacings; Table S2: *R*$_w$ values of refined models in the chain packing search; Table S3: Fractional atomic coordinates of the final crystal structure; Table S4: Observed and calculated structure factor amplitudes of the final structure.

Author Contributions: Conceptualization, T.Y. and K.O.; sample preparation and X-ray diffraction measurement, K.O.; crystal structure analysis, T.Y.; theoretical calculations, T.U.; writing—review and editing, T.Y. All authors have read and agreed to the published version of the manuscript.

Conflicts of Interest: The authors declare no conflict of interest.

References

1. Binnewerg, B.; Schubert, M.; Voronkina, A.; Muzychka, L.; Wysokowski, M.; Petrenko, I.; Djurovic, M.; Kovalchuk, V.; Tsurkan, M.; Martinovic, R.; et al. Marine biomaterials: Biomimetic and pharmacological potential of cultivated *Aplysina aerophoba* marine demosponge. *Mater. Sci. Eng. C* **2020**, *109*, 110566–110577. [CrossRef] [PubMed]
2. Muzzarelli, R.A.A. *Chitin*; Pergamon Press: Oxford, UK, 1977.
3. Kurita, K.; Sannan, T.; Iwakura, Y. Studies on chitin. VI. Binding of metal cations. *J. Appl. Polym. Sci.* **1979**, *23*, 511–515. [CrossRef]
4. Takeshita, S.; Zhao, S.; Malfait, W.J.; Koebel, M.M. Chemistry of chitosan aerogels: Three-dimensional pore control for tailored applications. *Angew. Chem. Int. Ed.* **2020**, *60*, 9828–9851. [CrossRef] [PubMed]
5. Ohkawa, K.; Minato, K.; Kumagai, G.; Hayashi, S.; Yamamoto, H. Chitosan nanofiber. *Biomacromolecules* **2006**, *7*, 3291–3294. [CrossRef] [PubMed]
6. Elsabee, M.Z.; Naguib, H.F.; Morsi, R.E. Chitosan based nanofibers, review. *Mater. Sci. Eng. C* **2012**, *32*, 1711–1726. [CrossRef]
7. AL-Jbour, N.D.; Beg, M.D.; Gimbun, J.; Alam, A. An overview of chitosan nanofibers and their applications in the drug delivery process. *Curr. Drug Deliv.* **2019**, *16*, 272–294. [CrossRef]
8. Horzum, N.; Boyaci, E.; Eroglu, A.E.; Shahwan, T.; Demir, M.M. Sorption efficiency of chitosan nanofibers toward metal ions at low concentrations. *Biomacromolecules* **2010**, *11*, 3301–3308. [CrossRef]
9. Min, L.L.; Zhong, L.B.; Zheng, Y.M.; Liu, Q.; Yuan, Z.H.; Yang, L.M. Functionalized chitosan electrospun nanofiber for effective removal of trace arsenate from water. *Sci. Rep.* **2016**, *6*, 32480. [CrossRef]
10. Clark, G.L.; Parker, E.A. An X-ray diffraction study of the action of liquid ammonia on cellulose and its derivatives. *J. Phys. Chem.* **1937**, *41*, 777–786. [CrossRef]
11. Ogawa, K.; Hirano, S.; Miyanishi, T.; Yui, T.; Watanabe, T. A new polymorph of chitosan. *Macromolecules* **1984**, *17*, 973–975. [CrossRef]
12. Yui, T.; Imada, K.; Okuyama, K.; Obata, Y.; Suzuki, K.; Ogawa, K. Molecular and crystal structure of the anhydrous form of chitosan. *Macromolecules* **1994**, *27*, 7601–7605. [CrossRef]
13. Okuyama, K.; Noguchi, K.; Miyazawa, T.; Yui, T.; Ogawa, K. Molecular and crystal structure of hydrated chitosan. *Macromolecules* **1997**, *30*, 5849–5855. [CrossRef]
14. Okuyama, K.; Noguchi, K.; Hanafusa, Y.; Osawa, K.; Ogawa, K. Structural study of anhydrous tendon chitosan obtained via chitosan/acetic acid complex. *Int. J. Biol. Macromol.* **1999**, *26*, 285–293. [CrossRef]
15. Ogawa, Y.; Kimura, S.; Wada, M.; Kuga, S. Crystal analysis and high-resolution imaging of microfibrillar α-chitin from *Phaeocystis*. *J. Struct. Biol.* **2010**, *171*, 111–116. [CrossRef]
16. Ogawa, K.; Oka, K.; Miyanishi, T.; Hirano, S. X-ray Diffraction Study on Chitosan-Metal Complexes. In *Chitin, Chitosan, and Related Enzymes*; Zikakis, J.P., Ed.; Academic Press: London, UK, 1984; pp. 327–345.
17. Domard, A. pH and c.d. measurements on a fully deacetylated chitosan: Application to Cu(II)—Polymer interactions. *Int. J. Biol. Macromol.* **1987**, *9*, 98–104. [CrossRef]

18. Schlick, S. Binding sites of Cu^{2+} in chitin and chitosan. An electron spin resonance study. *Macromolecules* **1986**, *19*, 192–195. [CrossRef]

19. Lertworasirikul, A.; Yokoyama, S.; Noguchi, K.; Ogawa, K.; Okuyama, K. Molecular and crystal structures of chitosan/HI type I salt determined by X-ray fiber diffraction. *Carbohydr. Res.* **2004**, *339*, 825–833. [CrossRef] [PubMed]

20. Ogawa, K.; Oka, K.; Yui, T. X-ray study of chitosan-transition metal complexes. *Chem. Mater.* **1993**, *5*, 726–728. [CrossRef]

21. Rhazi, M.; Desbrières, J.; Tolaimate, A.; Rinaudo, M.; Vottero, P.; Alagui, A.; El Meray, M. Influence of the nature of the metal ions on the complexation with chitosan. *Eur. Polym. J.* **2002**, *38*, 1523–1530. [CrossRef]

22. Wang, X.; Du, Y.; Liu, H. Preparation, characterization and antimicrobial activity of chitosan–Zn complex. *Carbohydr. Polym.* **2004**, *56*, 21–26. [CrossRef]

23. Zhai, X.; Sun, C.; Li, K.; Guan, F.; Liu, X.; Duan, J.; Hou, B. Synthesis and characterization of chitosan–zinc composite electrodeposits with enhanced antibacterial properties. *RSC Adv.* **2016**, *6*, 46081–46088. [CrossRef]

24. Arnott, S.; Scott, W.E. Accurate X-ray diffraction analysis of fibrous polysaccharides containing pyranose rings. Part I. The linked-atom approach. *J. Chem. Soc. Perkin Trans. 2* **1972**, *3*, 324–335. [CrossRef]

25. Smith, P.J.C.; Arnott, S. LALS: A linked-atom least-squares reciprocal-space refinement system incorporating stereochemical restraints to supplement sparse diffraction data. *Acta Crystallogr. Sect. A* **1978**, *34*, 3–11. [CrossRef]

26. Rappe, A.K.; Casewit, C.J.; Colwell, K.S.; Goddard, W.A.; Skiff, W.M. UFF, a full periodic table force field for molecular mechanics and molecular dynamics simulations. *J. Am. Chem. Soc.* **1992**, *114*, 10024–10035. [CrossRef]

27. Rappe, A.K.; Colwell, K.S.; Casewit, C.J. Application of a universal force field to metal complexes. *Inorg. Chem.* **1993**, *32*, 3438–3450. [CrossRef]

28. Deria, P.; Gomez-Gualdron, D.A.; Hod, I.; Snurr, R.Q.; Hupp, J.T.; Farha, O.K. Framework-topology-dependent catalytic activity of zirconium-based (porphinato)zinc(II) MOFs. *J. Am. Chem. Soc.* **2016**, *138*, 14449–14457. [CrossRef]

29. Zarabadi-Poor, P.; Marek, R. In silico study of (Mn, Fe, Co, Ni, Zn)-btc metal–organic frameworks for recovering xenon from exhaled anesthetic gas. *ACS Sustain. Chem. Eng.* **2018**, *6*, 15001–15006. [CrossRef]

30. Stewart, J.J. Optimization of parameters for semiempirical methods V: Modification of NDDO approximations and application to 70 elements. *J. Mol. Model.* **2007**, *13*, 1173–1213. [CrossRef]

31. Amin, E.A.; Truhlar, D.G. Zn coordination chemistry: Development of benchmark suites for geometries, dipole moments, and bond dissociation energies and their use to test and validate density functionals and molecular orbital theory. *J. Chem. Theory Comput.* **2008**, *4*, 75–85. [CrossRef]

32. Narayanan, V.V.; Gopalan, R.S.; Chakrabarty, D.; Mobin, S.M.; Mathur, P. Crystal structure and energy optimization of dichloro-bis(ethylanthranilatonicotinamide)zinc(II). *J. Chem. Crystallogr.* **2011**, *41*, 801–805. [CrossRef]

33. Romero, M.J.; Suarez, V.; Fernandez-Farina, S.; Maneiro, M.; Martinez-Nunez, E.; Zaragoza, G.; Gonzalez-Noya, A.M.; Pedrido, R. Effect of the metal ion on the enantioselectivity and linkage isomerization of thiosemicarbazone helicates. *Chem. Eur. J.* **2017**, *23*, 4884–4892. [CrossRef] [PubMed]

34. Pinheiro, P.S.M.; Rodrigues, D.A.; Sant'Anna, C.M.R.; Fraga, C.A.M. Modeling zinc-oxygen coordination in histone deacetylase: A comparison of semiempirical methods performance. *Int. J. Quantum Chem.* **2018**, *118*, e25720. [CrossRef]

35. Frisch, M.J.; Trucks, G.W.; Schlegel, H.B.; Scuseria, G.E.; Robb, M.A.; Cheeseman, J.R.; Scalmani, G.; Barone, V.; Mennucci, B.; Petersson, G.A.; et al. *Gaussian 09, Revision C. 01*; Gaussian Inc.: Wallingford, UK, 2009.

36. Schrödinger LLC. *The PyMOL Molecular Graphics System, ver. 1.7.1*; Schrödinger LLC: New York, NY, USA, 2014.

37. Gomes, J.R.B.; Jorge, M.; Gomes, P. Interaction of chitosan and chitin with Ni, Cu and Zn ions: A computational study. *J. Chem. Thermodyn.* **2014**, *73*, 121–129. [CrossRef]

38. Hennings, E.; Schmidt, H.; Voigt, W. Crystal structures of $ZnCl_2 \cdot 2.5H_2O$, $ZnCl_2 \cdot 3H_2O$ and $ZnCl_2 \cdot 4.5H_2O$. *Acta Crystallogr. Sect. Sect. E Struct. Rep. Online* **2014**, *70*, 515–518. [CrossRef]